Nanoscale

Accepted Manuscript

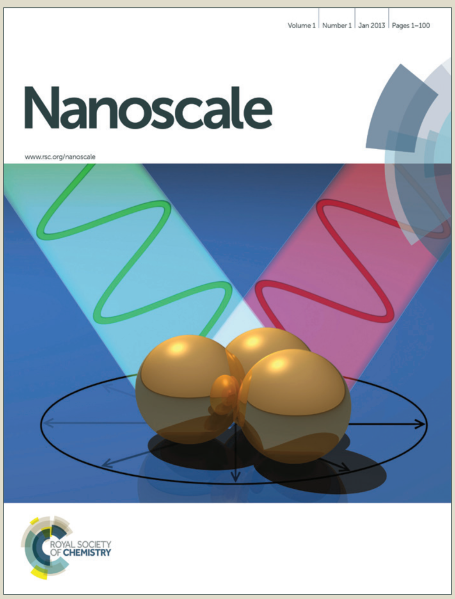

This is an *Accepted Manuscript*, which has been through the Royal Society of Chemistry peer review process and has been accepted for publication.

Accepted Manuscripts are published online shortly after acceptance, before technical editing, formatting and proof reading. Using this free service, authors can make their results available to the community, in citable form, before we publish the edited article. We will replace this *Accepted Manuscript* with the edited and formatted *Advance Article* as soon as it is available.

You can find more information about *Accepted Manuscripts* in the Information for Authors.

Please note that technical editing may introduce minor changes to the text and/or graphics, which may alter content. The journal's standard Terms & Conditions and the Ethical guidelines still apply. In no event shall the Royal Society of Chemistry be held responsible for any errors or omissions in this *Accepted Manuscript* or any consequences arising from the use of any information it contains.

ROYAL SOCIETY OF CHEMISTRY

www.rsc.org/nanoscale

Cobalt phosphate modified TiO_2 nanowire arrays as co-catalyst for solar water splitting

Guanjie Ai, Rong Mo, Hongxing Li,* Jianxin Zhong

Hunan Key Laboratory for Micro-Nano Energy Materials and Devices, School of Physics and Optoelectronics, Xiangtan University, Hunan 411105, P. R. China

email:hongxinglee@xtu.edu.cn

TOC graph

This paper demonstrates the improvement effect and mechanism insights of the Co-Pi electro-catalyst modified TiO_2 NWAs for solar water splitting.

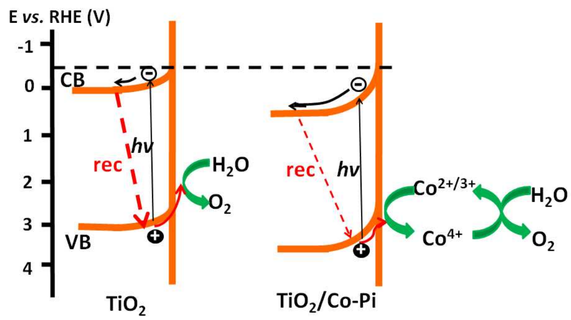

Abstract: The cobalt phosphate (Co-Pi) is photo-electrodeposited on the TiO_2 nanowire arrays in Co^{2+} containing phosphate buffer. The resulting composite photoanode shows generally enhanced photocurrent near the flat band potential region, and represents 2.3 times photoconversion efficiency improvement compared to the pristine TiO_2 in neutral electrolyte. A negative effect on the photocurrent generation is also observed when loading TiO_2 with relatively thick Co-Pi layer, which is demonstrated to be due to the poor photohole transfer kinetics in the Co-Pi layer. Moreover, we find that the Co-Pi can facilitate the photoelectrochemical performance of TiO_2 over a wide range of pH value from 1-14. This improved activity is studies in detail by optical and electrochemical analysis. It is suggested that the overpotential demanding water oxidation reaction is changed into a facile pathway by the Co-based electro-catalyst. At the same time, the more significant band bending is induced by

Nanoscale Accepted Manuscript

the Co-Pi catalyst to decrease the charge recombination. This work provides a feasible route to reduce of the external power needed to drive water splitting by the coupling of electro-catalyst with photo-catalyst as well as important mechanism insights for other Co-Pi modified photoelectrodes for solar-driven water splitting.

Introduction

The photoelectrochemical (PEC) splitting of water into hydrogen and oxygen is a nice duplication of the nature photosynthesis which collects the energy of sunlight and stores it in the form of chemical bonds. TiO_2 is one of the most extensively studied semiconductor materials for solar water splitting due to its excellent chemical stability, non-toxicity and earth abundance.[1-5] Especially, the energy band position (-0.29 V *vs.* RHE of conduction band edge and 2.91 V *vs.* RHE of the valence band edge) endues TiO_2 with the latent capacity for full solar-driven water splitting.[6, 7] The water splitting process involves two complicated multi-electron half reactions ($2H_2O \rightarrow O_2 + 4H^+ + 4e^-$, E^θ= 1.23 V *vs.* RHE; $4H^+ + 4e^- \rightarrow 2H_2$, E^θ= 0 V *vs.* RHE). Studies have indicated that the reactions between photogenerated holes and water molecules mainly limit the performance of PEC water splitting, as it generally occurs at a significant overpotential for the removal of a total of four electrons and four protons from two water molecules to form one O_2 molecule.[8-10] Therefore, even though the much more positive valence band edge of TiO_2 than the required potential for water oxidation thermodynamically, the water oxidation by photogenerated valence band holes is kinetically inefficient, and additional anodic bias are typically required before significant PEC water splitting is observed.[11] At the same time, the slow water oxidation reaction induces the large accumulation of photoholes at the electrode/electrolyte interface thus aggravates the electron-hole recombination and other side reactions.[12]

Catalyst is a fine-tuned molecular machinery which can change the reaction mechanism thus reduce the reaction energy barrier to boost the chemical reaction rate.[13, 14] Integration of oxygen evolution electro-catalyst with a photon-absorbing substrate therefore is a promising approach to reduce the external power needed to

Nanoscale Accepted Manuscript

drive the catalyst's electrolysis chemistry and improve the overall solar conversion efficiency. Considerable efforts have been devoted to develop suitable water oxidation electro-catalyst for photoelectrode.[15-21] Recently, the amorphous cobalt-phosphate (Co-Pi) emerges to be an attractive candidate catalyst material.[21-25] Compared to the precious metal (Ru, Ir) or metal oxide (RuO_2, IrO_x), extreme pH conditions required spinel and perovskite metal oxides oxygen evolution catalyst, Co-Pi possesses much advantages such as its earth abundant reserve, self-healing feature,[26] and functionality under benign conditions.[27] This active catalyst is believed to have a cubane structure resembling the oxygen-evolving complex of photosystem II.[28] Many semiconductor materials have been coupled with the Co-Pi electro-catalyst to exploit its merit of as co-catalyst.[29-33] For example, Steinmiller et al. reported that the Co-Pi modified ZnO photoanode shown improved PEC behavior with negatively shifted photocurrent onset potential and generally enhanced anodic photocurrent in the whole bias range.[34] Unfortunately, the Co-Pi does not always represents the enhancement effect on PEC performance of light-absorption substrates. For example, Bledowski reported the Co-Pi decorated TiO_2-C_3N_4 for PEC water splitting, the photocurrent enhancement of which was limited only in a certain bias range.[35] And the catalyst amount dependent PEC performance of the Co-Pi modified W-doped $BiVO_4$ was found in the report of Ye et al.[36]

Therefore, for the better utilization of the positive catalytic effect of the Co-Pi for semiconductor photoanode, the certainty about the microscopic identity of the catalyst appears to be significantly in request. While several reports[37-40] have confronted this issue, a generally acceptable nature interpretation of the Co-Pi electro-catalyst on photoanode substrate is far from satisfaction. For example, the creation of interface states by the Co-Pi deposition was introduced to explain the inconsistent catalytic effect of the Co-Pi on WO_3 when the applied bais varied form near flat band potential to more positive bias.[37] However, Zhong et al. identified an O_2 evolution kinetic limitation of the Co-Pi catalyst, which would be largely overcome by more sparse deposition of Co-Pi on photoanode.[38] A similar results of a related catalysts modified Fe_2O_3 also was reported that the amount reduction of $Ni(OH)_2$ catalyst would

Nanoscale Accepted Manuscript

surmount the negative catalytic effect, while the slow formation of the active catalytic species (Ni^{4+}) was demonstrated to explain the catalytic mechanism.[41] In contrast, Klahr et al. reported continual PEC improvement with increasing Co-Pi thickness on Fe_2O_3.[39] Additionally, another study indicated that Co-Pi did not directly participate in water-oxidation reaction but instead played an indirect role by inducing additional band bending for photoanode semiconductor to reduce electron-hole recombination.[42]

In this work, we report the co-catalytic effect as well as the mechanism insights of the Co-Pi electro-catalyst modified TiO_2 nanowire array photoanode. It is found that the anodic photocurrent of the TiO_2 electrode is generally improved by a sparse Co-Pi catalyst loading with its effect more pronounced when the band bending is less significant, and the solar-to-hydrogen conversion efficiency is enhanced by 2.3 times compared to its parent TiO_2 photoanode. A negative effect on the photocurrent generation is also observed when loading TiO_2 with thick Co-Pi catalyst, which is proposed to be due to the poor hole transfer kinetics of the Co-Pi layer. Finally, we demonstrate that the Co-Pi can facilitate the photoelectrochemical performance of TiO_2 over a wide range of pH value from 1-14. Based on a detailed electrochemical analysis and the predecessors' initiations, a plausible interpretation of the co-catalytic mechanism is proposed. This work provides a feasible route for the solar energy conversion efficiency improvement by coupling of the electro-catalyst with photocatalyst as well as important mechanism insights for other Co-Pi modified photoelectrodes for solar water oxidation.

Results and discussion

Nanoscale Accepted Manuscript

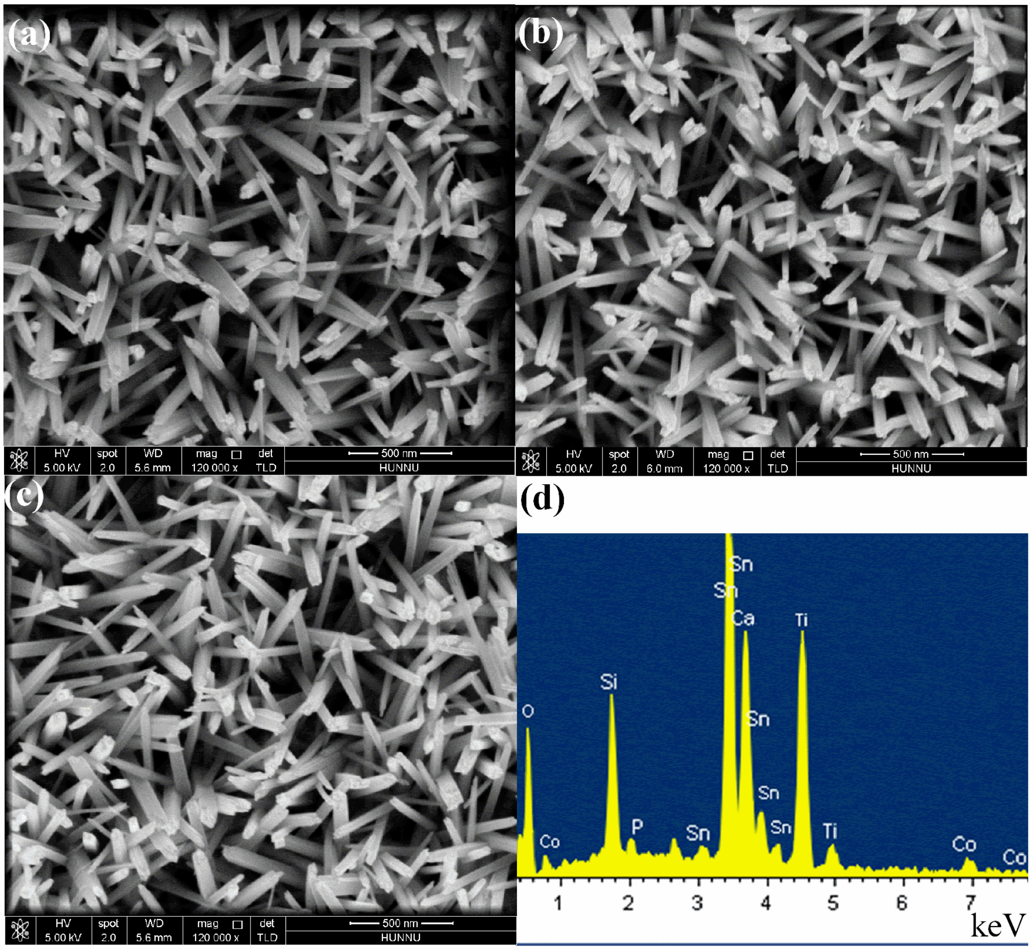

Fig. 1. SEM images of (a) pristine TiO_2, and the TiO_2 with (b) 10 uC cm^{-2} Co-Pi deposition and (c) 1 mC cm^{-2} Co-Pi deposition. (d) EDS spectra collected from TiO_2/Co-Pi (1 mC cm^{-2}) sample.

The TiO_2 nanowire array electrodes used in this work were grown on fluorine-doped tin oxide glass (FTO) substrates by hydrothermal method reported elsewhere (methods, see supporting information).[43] The TiO_2 nanowires are tetragonal in shape with diameter of ~75 nm (Fig. 1a). Co-Pi catalyst was decorated on the TiO_2 by photo-assisted electrodeposition in Co^{2+} containing phosphate buffer with the amount controlled by varying the quantity of electric charge passed through the external circuit. The white TiO_2 electrode becomes slightly dark green after 10 mC cm^{-2} Co-Pi deposition (see the inset in Fig. S1). Fig. 1b and Fig. 1c show the scanning electron microscope (SEM) images of the TiO_2 after the 10 uC cm^{-2} and 1 mC cm^{-2}

Nanoscale Accepted Manuscript

Co-Pi deposition respectively, which show no apparent morphology change compared to the pristine TiO_2 nanowire arrays but the images becomes somewhat brighter, suggesting that the catalysts make the surfaces more insulating and hence more susceptible to charging effects from the electron beam. Although the catalyst can not be resolved by the SEM measurement, the existences of Co and P element are confirmed by the energy dispersive spectroscopy (Fig. 1d). X-ray diffraction (XRD) spectra reveal the rutile crystal phase of the TiO_2 nanowire array (Fig. S2). The absence of (110) peak at 2θ of 27.4 indicates the vertically standing morphology of the nanowires, in consistent with the SEM observation. The indistinguishable XRD spectra of TiO_2/Co-Pi with pristine TiO_2 indicate the amorphous microstructure of Co-Pi catalyst. The UV-vis spectra of TiO_2 and TiO_2/Co-Pi show similar light absorption features, implying no additional band gap transition absorption induced by Co-Pi catalyst (Fig. S3). However, the Co-Pi catalyst layer may consume the incident light by nonproductive absorption, thus all the PEC test under light were carried out by backside illumination (from FTO to TiO_2) method.

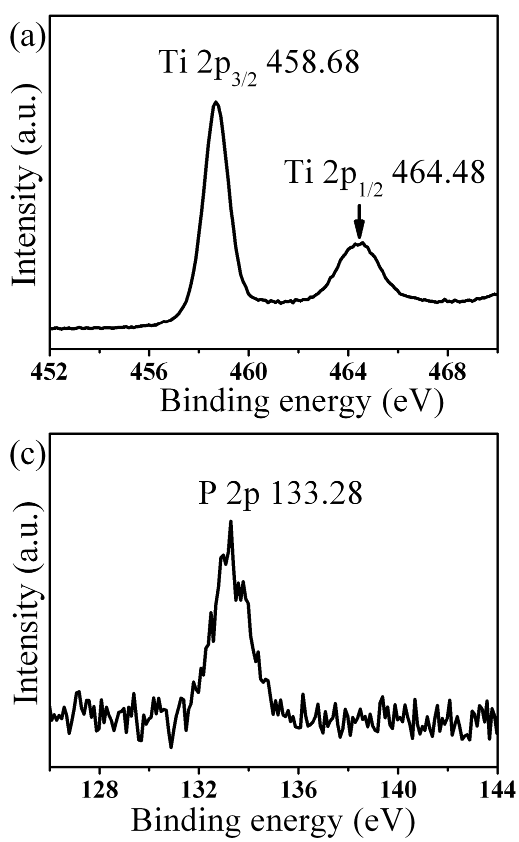

Nanoscale Accepted Manuscript

Fig. 2. High resolution XPS spectra of TiO_2/Co-Pi composite electrode: (a) Ti 2p, (b) O 1s, (c) P 2p, (d) Co 2p. The black curve is the experimental result. The red curve is the summation of the synthetic peaks in color curves.

The surface composition and elemental chemical state of the TiO_2/Co-Pi composite electrode were examined by X-ray photoelectron spectroscopy (XPS) as shown in Fig. 2. The strong Ti $2p_{3/2}$ and $2p_{1/2}$ XPS peaks at about 458.68 and 464.48 eV are attributed to Ti^{4+}.[44] The O 1s XPS spectra show a strong peak at ~529.98 eV and a shoulder peak at ~531.48 eV, which implies there are at least two kinds of O chemical states, including the crystal lattice oxygen (O_L) and hydroxyl oxygen (O_H) with increasing binding energy.[45] The binding energy of P 2p is at ~133.28 eV, which is characteristic of P in the phosphate group, confirming that P exists as the form of PO_4^{3-}.[21] The characteristic peaks of Co $2p_{3/2}$ and Co $2p_{1/2}$ at around 781.08 and 797.28 eV is in the typical range of Co^{2+} and Co^{3+} respectively.[21] The main Co $2p_{1/2}$ peak of Co^{3+} ions generally appears between 794.0 and 794.7 eV, and the shift of this peak to a higher binding energy is indicative of an increase in the Co^{2+}/Co^{3+} ratio in the sample.[46] We believe that the Co^{2+}/Co^{3+} ratio in the as-deposited Co-Pi catalyst is not as important as the total amount or nucleation density of the Co-Pi catalyst in affecting the overall catalytic ability, because the oxidation states of Co ions in the catalyst are supposed to continuously change in a cyclic manner ($Co^{2+/3+} \rightarrow Co^{4+} \rightarrow Co^{2+/3+}$) during the course of water oxidation.

Nanoscale Accepted Manuscript

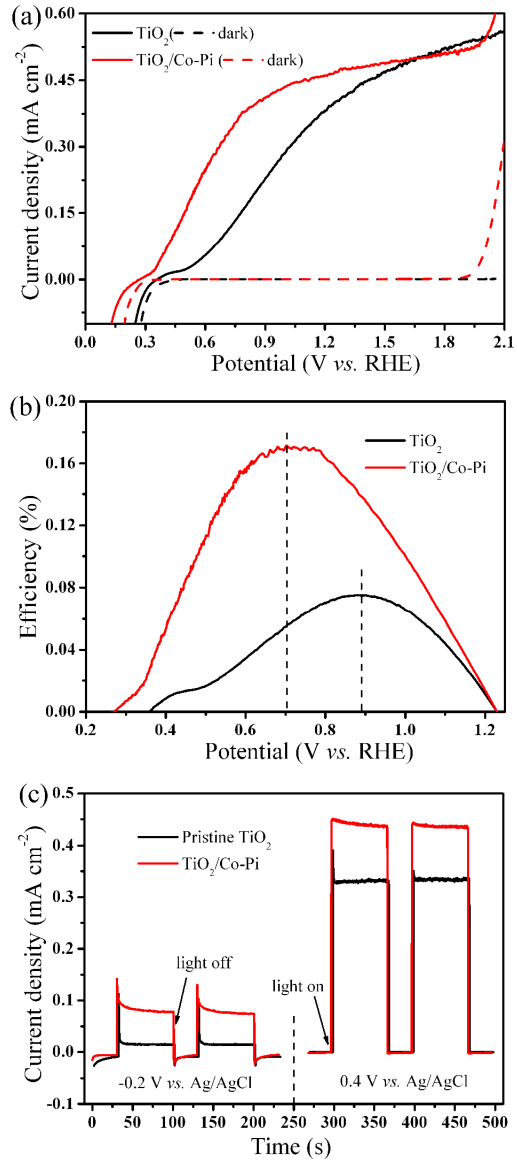

Fig. 3. PEC measurements of the TiO_2 and the parent TiO_2 with 10 uC cm^{-2} Co-Pi composite electrode in 0.1 M potassium phosphate electrolyte (pH=7). (a) Linear sweep voltammograms (*i-v* curves) under constant 1 sun illumination at scan rate of 25 mV s^{-1}, (b) calculated photoconversion efficiencies, (c) transient photocurrent densities measured at -0.2 V and 0.4 V *vs.* Ag/AgCl with chopped light illumination.

Fig. 3 compares the PEC properties of pristine TiO_2 and the same TiO_2 coated with 10 uC cm^{-2} Co-Pi catalyst measured in 0.1 M potassium phosphate electrolyte (pH=7). In Fig. 3a, the photocurrent of TiO_2 electrode is largely enhanced after the deposition of Co-Pi catalyst especially when the band bending is less significant. The

Nanoscale Accepted Manuscript

Mott-Schottky plots show that the pristine TiO_2 and composite TiO_2/Co-Pi electrodes have comparable flat band potentials under a certain frequency (Fig. S4). And no additional optical absorption by Co-Pi layer makes contribution to the enhanced photocurrent as evidenced by UV-vis spectra (Fig. S3) and the *i-v* curves of FTO/Co-Pi electrode (Fig. S5). Therefore, the observed photocurrent improvement can be attributed to the reduced electron-hole recombination rate near the flat band potential caused by Co-Pi catalytic effect.[34, 37] It is noteworthy that the catalytic effect for improving the photocurrent becomes less pronounced when the applied bias becomes more positive. This is because the increasing external bias can provide more powerful force to drive the electron-hole pair separation and water oxidation reaction even without the assistance of the electro-catalyst. In addition, we can observe that the photocurrent of TiO_2/Co-Pi electrode becomes even lower than that of the pristine TiO_2 when the external bias exceeds ~1.6 V *vs.* RHE. This critical potential shifts to a more negative value when coating TiO_2 with increased amount of Co-Pi catalyst, which is ascribed to the slow hole transfer kinetics in Co-Pi catalyst and will be discussed later.

Compared to the negative role of Co-Pi catalyst in enhancing the photoactivity of TiO_2 in high bias region, the photocurrent enhancement in low bias region is more attractive since the high photocurrent at small bias potential can reduce the external power needed to drive water splitting and, thus, increases the overall efficiency of PEC hydrogen generation. The photoconversion (i.e., photon-to-hydrogen) efficiencies (η) of the TiO_2 and TiO_2/Co-Pi photoanodes are deduced from Fig. 3a using the following equation:[47]

$$\eta=I(E^{\theta}_{rev}-V)/J_{light}$$

where I is the photocurrent density (mA cm^{-2}) at the measured bias, E^{θ}_{rev} is the standard reversible potential which is 1.23 V *vs.* RHE for the water-splitting reaction at pH 0, and V is the applied bias potential *vs.* RHE. J_{light} is the irradiance intensity (100 mW cm^{-2}). Fig. 3b presents the plots of the photoconversion efficiencies as a function of the applied bias. The pristine TiO_2 sample exhibits an optimal conversion efficiency of 0.075% at ~0.9 V *vs.* RHE. Significantly, TiO_2/Co-Pi photoanode

Nanoscale Accepted Manuscript

achieves the highest efficiency of 0.17 % at a relatively low bias of ~0.7 V *vs.* RHE. The more than 2 times photoconversion efficiency enhancement at smaller external bias directly demonstrates the coupling of Co-Pi with TiO_2 is an available way for higher PEC behavior of TiO_2.

Fig. 3c displays the transient photocurrent curves (*i-t* curves) collected under chopped light illumination. At -0.2 V vs. Ag/AgCl, the TiO_2/Co-Pi and the pristine TiO_2 photoanodes both show spikes within the first second of irradiation. These spikes can be attributed to the charge carrier accumulation at the electrode-electrolyte interface due to the slow oxygen evolution kinetics or oxidization of trap states on the surface and in the bulk by charge carriers.[48] However, the steady-state photocurrent density of TiO_2/Co-Co-Pi photoanode is retained 6 times more than that of the parent TiO_2 photoanode, which is ascribed to the relieved charge accumulation and boosted water oxidation reaction due to the Co-Pi catalyst. When the applied bais is 0.4 V *vs.* Ag/AgCl, the difference between photocurrent generated from the TiO_2/Co-Pi and bare TiO_2 is reduced, which is in accordance with the results in Fig. 3a. While spikes are still exhibited by the pristine TiO_2 upon illumination, only negligible reduction can be identified by TiO_2/Co-Pi electrode. The slight decrease of the initial photocurrent can be partially attributed to cobalt oxidation, which is an essential step in the catalytic water oxidation mechanism.

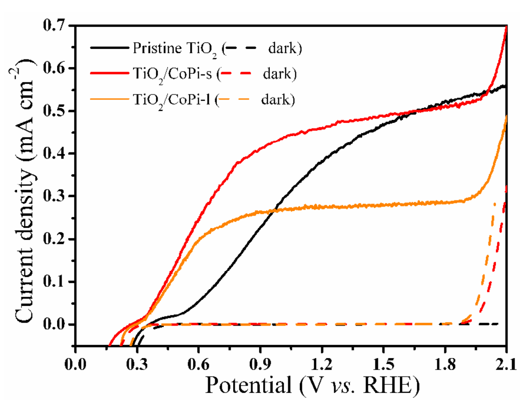

Fig. 4. *i-v* curves of TiO_2 coated with different amount of Co-Pi catalyst measured in 0.1 M potassium phosphate electrolyte (pH=7) under constant 1 sun illumination at scant rate of 25 mV s^{-1}.

Nanoscale Accepted Manuscript

As mentioned above, a negative effect on photocurrent generation may be induced by Co-Pi catalyst in high bias region especially when the Co-Pi layer is thick. Fig. 4 shows the *i-v* curves of the TiO_2 nanowire array electrode and the same TiO_2 coated with different amount of Co-Pi catalyst. The red line is for the TiO_2/Co-Pi with 10 uC cm^{-2} (referred as TiO_2/Co-Pi-s, small) and the orange line is for the one with 1 mC cm^{-2} (referred as TiO_2/Co-Pi-l, large) passed through the external bias during deposition. Obviously, the photocurrent plateau of TiO_2/Co-Pi-l is depressed at a relatively low level compared to that of parent TiO_2 and TiO_2/Co-Pi-s, with the photocurrent improvement restricted in the range of 0.2-0.95 V *vs.* RHE. Not like the TiO_2/Co-Pi-s, the anodic scanning photocurrents of TiO_2/Co-Pi-l show strong scan rate dependence in the cyclic voltammograms (Fig. S6). This result implies that assignable photocurrent enhancement of TiO_2/Co-Pi-l is coming from the charging effect, where the TiO_2/Co-Pi-l electrode functioned as a pseudocapacitor electrode. A similar Co-Pi thickness dependence of the photocurrent has also been observed previously in Fe_2O_3/Co-Pi photoanode.[38] Based on the proposed catalytic mechanism that involves the $Co^{2+/3+} \rightarrow Co^{4+} \rightarrow Co^{2+/3+}$ reaction circle by Surendranath et al.,[49] a plausible explanation for negative influence on photocurrent generation caused by thick Co-Pi layer is given as following. The catalytic water oxidation reaction is happened at the Co/electrolyte interface. If the Co-Pi layer is extremely thin (e.g., only one layer $Co^{2+/3+}$ linked to the surface of TiO_2 by phosphate groups), the directly linked $Co^{2+/3+}$ on TiO_2 surface is easy to capture the photoholes to produce active catalytic species (Co^{4+})[50] for water oxidation. However, when the Co-Pi layer becomes thicker, the photoholes must be transferred to the Co-Pi/electrolyte interface through many in-between Co-Pi molecules. The slow hole transfer rate in the intermediate Co-Pi may be due to the thermodynamically difficult reaction between Co ions with adjacent valence (e.g., Co^{4+} and Co^{3+}), which is responsible for the depressed photocurrent. As a result, the holes are accumulated at the TiO_2/Co-Pi interface and accelerate the electron-hole recombination in return.

Nanoscale Accepted Manuscript

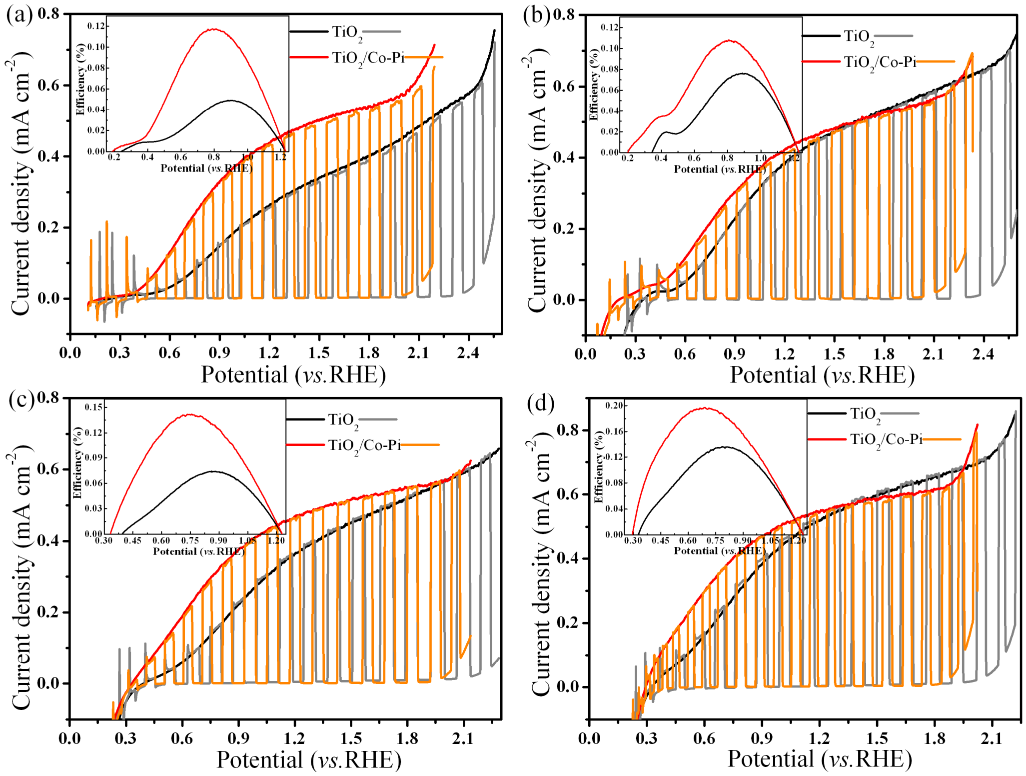

Fig. 5. *i*-*v* curves of the pristine TiO_2 and TiO_2/Co-Pi composite electrode in 0.1 M potassium phosphate electrolyte with pH value adjusted to (a) pH=1, (b) pH=4, (c) pH=10, (d) pH=14 under constant and chopped 1 sun illumination. The insets are the photoconversion efficiency curves calculated from the corresponding *i*-*v* curves.

The above PEC measurement results demonstrate the availability to obtain PEC performance improvement for TiO_2 in neutral electrolytes by a sparse Co-Pi decoration, further, we investigate this positive catalytic effect in acid and alkaline electrolytes. It should be mentioned that to keep the same ionic environment (e.g., ionic species, ionic strength) as far as possible, four equal 0.1 M potassium phosphate electrolytes were prepared and the pH value of them were accurately adjusted to 1, 4, 10, 14 respectively by concentrated H_2SO_4 or KOH aqueous solution. As shown in Fig. 5, the photocurrent densities of the parent TiO_2 nanowire array electrodes in different pH value electrolyte are all improved after the modification of Co-Pi catalyst in the low bias potential region. The photoconversion efficiencies (inset in each *i*-*v* curve panel in Fig. 5) are improved by 1.98, 1.42, 1.92, 1.46 times more than that of

Nanoscale Accepted Manuscript

the corresponding parent TiO_2 electrode in pH 1, 4, 10 and 14 electrolytes, respectively. These results indicate that the Co-Pi catalyst can facilitate the PEC behavior of TiO_2 over a wide range of pH value from 1-14. The enhancement in wide range pH value implies the promising applications of Co-Pi modification for other light absorption substrates in various pH electrolyte.

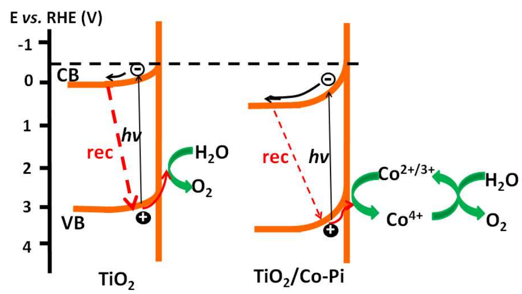

Fig. 6. Schematic band diagrams illustrating the proposed catalytic mechanism of Co-Pi on TiO_2 for PEC water oxidation.

Fig. 6 illustrates the proposed explanation for the improved PEC performance of the TiO_2 after the Co-Pi modification. As the light absorption consideration has been excluded, the enhanced photocurrent can be mainly attributed to the reduced charge carrier recombination which is induced by several reasons. First, as an oxygen evolution catalyst, the Co-Pi can catalyze the water electrolysis process to proceed at a low overpotential by changing the reaction pathway.[51] When combined with the TiO_2, the Co-Pi use the valence band photohole of the TiO_2 to drive $Co^{2+/3+} \rightarrow Co^{4+} \rightarrow Co^{2+/3+}$ circular catalytic reactions, accompanied by the fast output of photohole from TiO_2 to water molecule (i. g., water oxidation) if the Co-Pi layer is thin enough. Thus, the relieved charge accumulation at the electrode/electrolyte decreases the electron-hole recombination rate and leads to enhanced overall PEC performance. Second, the additional band bending at the electrode/electrolyte interface may be created by the Co-Pi catalyst, which can also reduce the surface charge recombination.[52] In Fig. S4, the Mott-Schottky plot of TiO_2/Co-Pi exhibits a larger slope compared to that of the parent TiO_2 electrode, indicating the decreased donor density in TiO_2/Co-Pi.[53] The decreased donor density may be due to the

Nanoscale Accepted Manuscript

formation of TiO_2/Co-Pi heterojunction which depletes of electrons in the TiO_2 conduction band and results in the additional band bending.[54]

Summary

We have studied the co-catalytic effect by coupling the Co-Pi oxygen evolution electro-catalyst with TiO_2 photocatalyst for solar water splitting. Electrochemical analyst demonstrates that the PEC performance of TiO_2 is substantially improved by relatively sparse Co-Pi modification especially in the low bias region. It is also observed that the increasing of the Co-Pi amount have negative effect on the photocurrent generation, which is demonstrated to be due to the poor photohole transfer kinetics in the Co-Pi layer. Moreover, we find that the Co-Pi can facilitate the PEC performance of TiO_2 over a wide range of pH value from 1-14. The enhanced PEC behaviors are benefited from the reduced change recombination caused by Co-Pi catalyst due to the changed water oxidation mechanism and enhanced band bending. This work provides a feasible route to reduce of the external power needed to drive water splitting by the coupling of electro-catalyst with photocatalyst as well as important mechanism insights for other Co-Pi modified photoelectrodes for solar-driven water splitting.

Acknowledgements

We thank the financial support of the National Natural Science Foundation of China (Grant no. 51202208, 51172191, and 11274264), The Project Supported by Scientific Research Fund of Hunan Provincial Education Department (Grant no. 12B129), National Basic Research Program of China (no. 2012CB921303) and the Program for Changjiang Scholars and Innovative Research Team in University (IRT13093). We also thank Professor Hong Jin Fan of Nanyang Technological University for his useful suggestions and discussions.

References:

1. B. Lu, C. Zhu, Z. Zhang, W. Lan and E. Xie, *J. Mater. Chem.*, 2012, **22**,

Nanoscale Accepted Manuscript

1375-1379.

2. C. Dette, M. A. Pérez-Osorio, C. S. Kley, P. Punke, C. E. Patrick, P. Jacobson, F. Giustino, S. J. Jung and K. Kern, *Nano Lett.*, 2014, **14**, 6533-6538.

3. S. Lee, S. Park, G. S. Han, D. H. Kim, J. H. Noh, I. S. Cho, H. S. Jung and K. S. Hong, *Nanoscale*, 2014, **6**, 8649.

4. G. Ai, R. Mo, H. Xu, Q. Chen, S. Yang, H. Li and J. Zhong, *J. Power Sources*, 2015, **280**, 5-11.

5. G. Zhang, H. Duan, B. Lu and Z. Xu, *Nanoscale*, 2013, **5**, 5801-5808.

6. Y. Xu and M. A. A. Schoonen, *Am. Mineral*, 2000, **85**, 543-556.

7. Z. Zhang and J. T. Yates, *Chem. Rev.*, 2012, **112**, 5520-5551.

8. J. Barber, *Chem. Soc. Rev.*, 2009, **28**, 185-196.

9. Y. Zhang, C. Zhao, X. Dai, H. Lin, B. Cui and J. Li, *J. Power Sources*, 2013, **243**, 908-912.

10. M. D. Kärkäs, O. Verho, E. V. Johnston and B. Åkermark, *Chem. Rev.*, 2014, **114**, 11863-12001.

11. I. Paramasivam, H. Jha, N. Liu and P. Schmuki, *Small*, 2012, **8**, 3073-3103.

12. X. Tong, P. Yang, Y. Wang, Y. Qin and X. Guo, *Nanoscale*, 2014, **6**, 6692-6700.

13. M. Yagi and M. Kaneko, *Chem. Rev.*, 2001, **101**, 21-36.

14. M. W. Kanan, Y. Surendranath and D. G. Nocera, *Chem. Soc. Rev.*, 2009, **38**, 109-114.

15. M. Seol, J. Jang, S. Cho, J. S. Lee and K. Yong, *Chem. Mater.*, 2013, **25**, 184-189.

16. L. Ma, S. Sui and Y. Zhai, *J. Power Sources*, 2008, **177**, 470-477.

17. R. Al-Oweini, A. Sartorel, B. S. Bassil, M. Natali, S. Berardi, F. Scandola, U. Kortz and M. Bonchio, *Angew. Chem. Int. Ed.*, 2014, **53**, 11182-11185.

18. J. H. Kim, J. W. Jang, H. J. Kang, G. Magesh, J. Y. Kim, J. H. Kim, J. Lee and J. S. Lee, *J. Catal.*, 2014, **317**, 126-134.

19. W. Ryu, Y. W. Lee, Y. S. Nam, D. Youn, C. B. Park and I. Kim, *J. Mater. Chem. A*, 2014, **2**, 5610-5615.

20. V. Kunz, V. Stepanenko and F. Wurthner, *Chem. Commun.*, 2015, **51**, 290-293.

Nanoscale Accepted Manuscript

21. M. W. Kanan and D. G. Nocera, *Science*, 2008, **321**, 1072-1075.

22. D. K. Zhong, J. Sun, H. Inumaru and D. R. Gamelin, *J. Am. Chem. Soc.*, 2009, **131**, 6086-6087.

23. Y. Li, L. Zhang, A. Torres-Pardo, J. M. González-Calbet, Y. Ma, P. Oleynikov, O. Terasaki, S. Asahina, M. Shima, D. Cha, L. Zhao, K. Takanabe, J. Kubota and K. Domen, *Nature Commun.*, 2013. DOI: 10.1038/ncomms3566.

24. T. Jin, P. Diao, Q. Wu, D. Xu, D. Hu, Y. Xie and M. Zhang, *Appl. Catal. B: Environ.*, 2014, **148-149**, 304-310.

25. J. Tian, H. Li, A. M. Asiri, A. O. Al-Youbi and X. Sun, *Small*, 2013, **9**, 2709-2714.

26. D. A. Lutterman, Y. Surendranath and D. G. Nocera, *J. Am. Chem. Soc.*, 2009, **131**, 3838-3839.

27. Y. Surendranath, M. W. Kanan and D. G. Nocera, *J. Am. Chem. Soc.*, 2010, **132**, 16501-16509.

28. M. W. Kanan, Y. Surendranath and D. G. Nocera, *Chem. Soc. Rev.*, 2009, **38**, 109-114.

29. S. K. Pilli, T. E. Furtak, L. D. Brown, T. G. Deutsch, J. A. Turner and A. M. Herring, *Energy Environ. Sci.*, 2011, **4**, 5028-5034.

30. G. M. Carroll, D. K. Zhong and D. R. Gamelin, *Energy Environ. Sci.*, 2015, **8**, 577-584.

31. D. Liu, L. Jing, P. Luan, J. Tang and H. Fu, *ACS Appl. Mater. Interfaces*, 2013, **5**, 4046-4052.

32. S. K. Pilli, T. G. Deutsch, T. E. Furtak, J. A. Turner, L. D. Brown and A. M. Herring, *Phys. Chem. Chem. Phys.*, 2012, **14**, 7032.

33. F. F. Abdi and R. van de Krol, *J. Phys. Chem. C*, 2012, **116**, 9398-9404.

34. E. M. P. Steinmiller and K. Choi, *Proc. Natl. Acad. Sci. U.S.A.*, 2009, **106**, 20633-20636.

35. M. Bledowski, L. Wang, A. Ramakrishnan, A. Bétard, O. V. Khavryuchenko and R. Beranek, *ChemPhysChem*, 2012, **13**, 3018-3024.

36. H. Ye, H. S. Park and A. J. Bard, *J. Phys. Chem. C*, 2011, **115**, 12464-12470.

Nanoscale Accepted Manuscript

37. J. A. Seabold and K. Choi, *Chem. Mater.*, 2011, **23**, 1105-1112.

38. D. K. Zhong and D. R. Gamelin, *J. Am. Chem. Soc.*, 2010, **132**, 4202-4207.

39. B. Klahr, S. Gimenez, F. Fabregat-Santiago, J. Bisquert and T. W. Hamann, *J. Am. Chem. Soc.*, 2012, **134**, 16693-16700.

40. H. T. W., *Nature Mater.*, 2014, **13**, 3-4.

41. G. Wang, Y. Ling, X. Lu, T. Zhai, F. Qian, Y. Tong and Y. Li, *Nanoscale*, 2013, **5**, 4129.

42. M. Barroso, A. J. Cowan, S. R. Pendlebury, M. Grätzel, D. R. Klug and J. R. Durrant, *J. Am. Chem. Soc.*, 2011, **133**, 14868-14871.

43. G. Ai, R. Mo, H. Xu, Q. Chen, S. Yang, H. Li and J. Zhong, *J. Appl. Phys.*, 2014, **116**, 174306.

44. R. Sanjinés, H. Tang, H. Berger, F. Gozzo, G. Margaritondo and F. Lévy, *J. Appl. Phys.*, 1994, **75**, 2945.

45. F. Cui, L. Xu, T. Cui, T. Yao, Jing Yu, Z. Xiao and S. Kening, *RSC Adv.*, 2014, **4**, 33408-33415.

46. K. J. McDonald and K. Choi, *Chem. Mater.*, 2011, **23**, 1686-1693.

47. J. Gan, L. Xihong and T. Yexiang, *Nanoscale*, 2014, **6**, 7142-7164.

48. G. Ai, R. Mo, Q. Chen, H. Xu, S. Yang, H. Li and J. Zhong, *RSC Adv.*, 2015, **5**, 13544-13549.

49. Y. Surendranath, M. W. Kanan and D. G. Nocera, *J. Am. Chem. Soc.*, 2010, **132**, 16501-16509.

50. J. G. McAlpin, Y. Surendranath, M. Dincă, T. A. Stich, S. A. Stoian, W. H. Casey, D. G. Nocera and R. D. Britt, *J. Am. Chem. Soc.*, 2010, **132**, 6882-6883.

51. P. Li, Z. Jin and D. Xiao, *J. Mater. Chem. A*, 2014, **2**, 18420-18427.

52. Z. Zhang and J. T. Yates, *Chem. Rev.*, 2012, **112**, 5520-5551.

53. M. Yang, B. Ding and J. Lee, *J. Power Sources*, 2014, **245**, 301-307.

54. M. Barroso, A. J. Cowan, S. R. Pendlebury, M. Grätzel, D. R. Klug and J. R. Durrant, *J. Am. Chem. Soc.*, 2011, **133**, 14868-14871.

Nanoscale Accepted Manuscript